

## NEUROSCIENCE

# Social place-cells in the bat hippocampus

David B. Omer, Shir R. Maimon, Liora Las,<sup>\*†</sup> Nachum Ulanovsky<sup>\*†</sup>

Social animals have to know the spatial positions of conspecifics. However, it is unknown how the position of others is represented in the brain. We designed a spatial observational-learning task, in which an observer bat mimicked a demonstrator bat while we recorded hippocampal dorsal-CA1 neurons from the observer bat. A neuronal subpopulation represented the position of the other bat, in allocentric coordinates. About half of these “social place-cells” represented also the observer’s own position—that is, were place cells. The representation of the demonstrator bat did not reflect self-movement or trajectory planning by the observer. Some neurons represented also the position of inanimate moving objects; however, their representation differed from the representation of the demonstrator bat. This suggests a role for hippocampal CA1 neurons in social-spatial cognition.

It is important for social animals to know the spatial position of conspecifics, for purposes of social interactions, observational learning, and group navigation. Decades of research on the mammalian hippocampal formation has revealed a set of spatial neurons that represent self-position and orientation, including place cells (1–3), grid cells (4–6), head-direction cells (7–9), and border/boundary cells (10–12). However, it remains unknown how the location of other animals is represented in the brain.

We designed an observational-learning task for Egyptian fruit bats (*Rousettus aegyptiacus*), which are highly social mammals that live in colonies with complex social structures (13). Bats were trained in pairs: In each trial, one bat (“observer”) had to remain stationary on a “start ball” and to observe and remember the flight trajectory of the other bat (“demonstrator”), which was flying roughly randomly to one of two landing balls (Fig. 1A, “demonstrator flying” in trials *i* and *j*). After a delay, the observer bat had to imitate the demonstrator bat and fly to the same landing ball to receive a reward (Fig. 1A, “observer flying,” and movies S1 and S2). This task had two key features: First, it required the observer to pay close attention to the demonstrator’s position and to hold this position in memory during the delay period (the average delay between the demonstrator’s return to the start ball and the observer’s takeoff was rather long:  $12.7 \pm 8.6$  s; mean  $\pm$  SD). Second, because the observer was stationary during the demonstrator’s flight, it allowed temporal dissociation between the effects of self-flights versus the flights of the other bat.

While the bats performed the task, we recorded the activity of 378 single neurons in the dorsal hippocampal area CA1 of four observer bats, using a wireless electrophysiology system (Fig. 1B) (14). For each neuron, we computed two firing-rate

maps: a “classical” map, based on the self-movement flight trajectories of the observer—the standard depiction for place cells (Fig. 1C, “Self,” left map for each neuron)—and a nonclassical map based on the spikes recorded from the observer’s neuron together with the demonstrator’s flight trajectories (Fig. 1C, “Demo,” right maps) (14). We focused our analysis on the two-dimensional horizontal projections because the bats’ flights were confined mostly to a narrow horizontal slab around the height of the landing balls (fig. S1). A subpopulation of hippocampal CA1 neurons encoded the position of the demonstrator-bat (Fig. 1C, cells 358, 254, 52, and 266—the right map in each example—and fig. S2). We termed these neurons “social place-cells.”

We classified 68 of the 378 recorded CA1 neurons (18.0%) as significant social place-cells—significantly encoding the position of the other bat—based on spatial information (95th percentile in a shuffling analysis) (14). Using the same criteria, 261 of the 378 recorded neurons (69.0%) significantly encoded the self-position of the observer bat when it was flying and were thus classified as place cells (Fig. 1D). Of the 261 place cells, 14.9% were also social place-cells. Conversely, of the 68 social place-cells, 57.4% (39 neurons) were also place cells (Fig. 1, C—cells 358, 254, 52—and D), whereas the remaining 29 social place-cells (42.6%) were not place cells. Most of these neurons (16 of 29 cells; 55.2%) became completely inactive during self-flights, although they encoded the conspecific’s position on interleaved demonstrator flights (examples are provided in Fig. 1C, cell 266, and fig. S2, cells 229 and 60).

This new type of social-spatial representation exhibited several features that were similar to the standard place cell representation: Both representations showed directional selectivity (Fig. 1E and fig. S3), and both place cells and social place-cells tiled space rather uniformly (Fig. 1F). However, we found also clear differences between the two representations: First, the firing rates of the social place-cells were significantly lower than for the classical place-cells (unpaired *t* test,  $P < 0.01$ ) (Fig. 1G) [firing-rates of classical place cells were

similar to our previous report from CA1 of flying bats (15)]. Second, in the 39 cells that encoded both self-position and conspecific position—we were both place cells and social place-cells—we found a wide range of correlation values between the representations for self and other. Some neurons exhibited high similarity between their place field and social place field (“congruent cells,” with positive correlations) (fig. S2, cells 68 and 45), whereas in other neurons, the place field and social place field were dissimilar (“noncongruent cells,” with negative correlations) (Fig. 1C, cells 358 and 254, and fig. S2, cell 242). Overall, we found a continuum from noncongruent to congruent representations (Fig. 1H, top histograms), but we also found a slight overrepresentation of congruent cells among higher-firing neurons (Fig. 1H, bottom, gray bars, and top right histogram). These data suggest partial remapping between the hippocampal representations of self-position and conspecific-position, which can be interpreted as reflecting the contextual difference between observing a conspecific versus self-movement.

Next, we sought to rule out the possibility that social place fields might result from the observer’s head movements during the demonstrator’s flights. We therefore recorded head acceleration and head azimuth using a nine-axis motion-sensor that was placed on the observer’s head (14). When the demonstrator bat was flying, the observer bat hardly moved its head: There was a lack of changes in head acceleration of the observer bat during the flights of the demonstrator bat (Fig. 2A, middle and bottom, gray areas). Consistent with this, in most of the demonstrator flights, the head azimuth of the observer changed by less than  $20^\circ$ , which is equivalent to a very small head movement of less than 6 mm (Fig. 2, B—black traces and rightmost *y* axis, in magenta—and C). Such small head movements did not modulate the firing of social place-cells outside the task (Fig. 2D). These bats have a wide visual field and no fovea (13) and hence did not need to move their head in order to track the demonstrator. However, in some of the demonstrator flights (35.4%), the observer bat did move its head more than  $20^\circ$  (the value of  $20^\circ$  corresponds roughly to  $\pm 1$  SD in azimuth) (Fig. 2, B, gray traces and C, gray vertical lines). These deviant flights might have potentially modulated the firing of the neurons. To rule out this possibility, we recomputed the social firing-rate maps after excluding the deviant flights and found that these maps were very similar to the original maps (Fig. 2, E, examples, and F, population analysis).

A second potential interpretation is that social place fields may reflect planning of the upcoming flight trajectory by the observer bat. To rule out this possibility, we conducted three analyses. (i) Trajectory planning by hippocampal cell assemblies has been linked to sharp-wave-ripples (SWRs) (16). We recorded the local field potential (LFP) in the observer bat, then detected SWRs (Fig. 2, G and H) and tested whether removing the observer flights that contained SWRs would affect social place fields (Fig. 2, I and J) (14). The removal of these flights hardly affected the social place field

Department of Neurobiology, Weizmann Institute of Science, Rehovot 76100, Israel.

\*These authors contributed equally to this work.

†Corresponding author. Email: nachum.ulanovsky@weizmann.ac.il (N.U.); liora.las@weizmann.ac.il (L.L.)

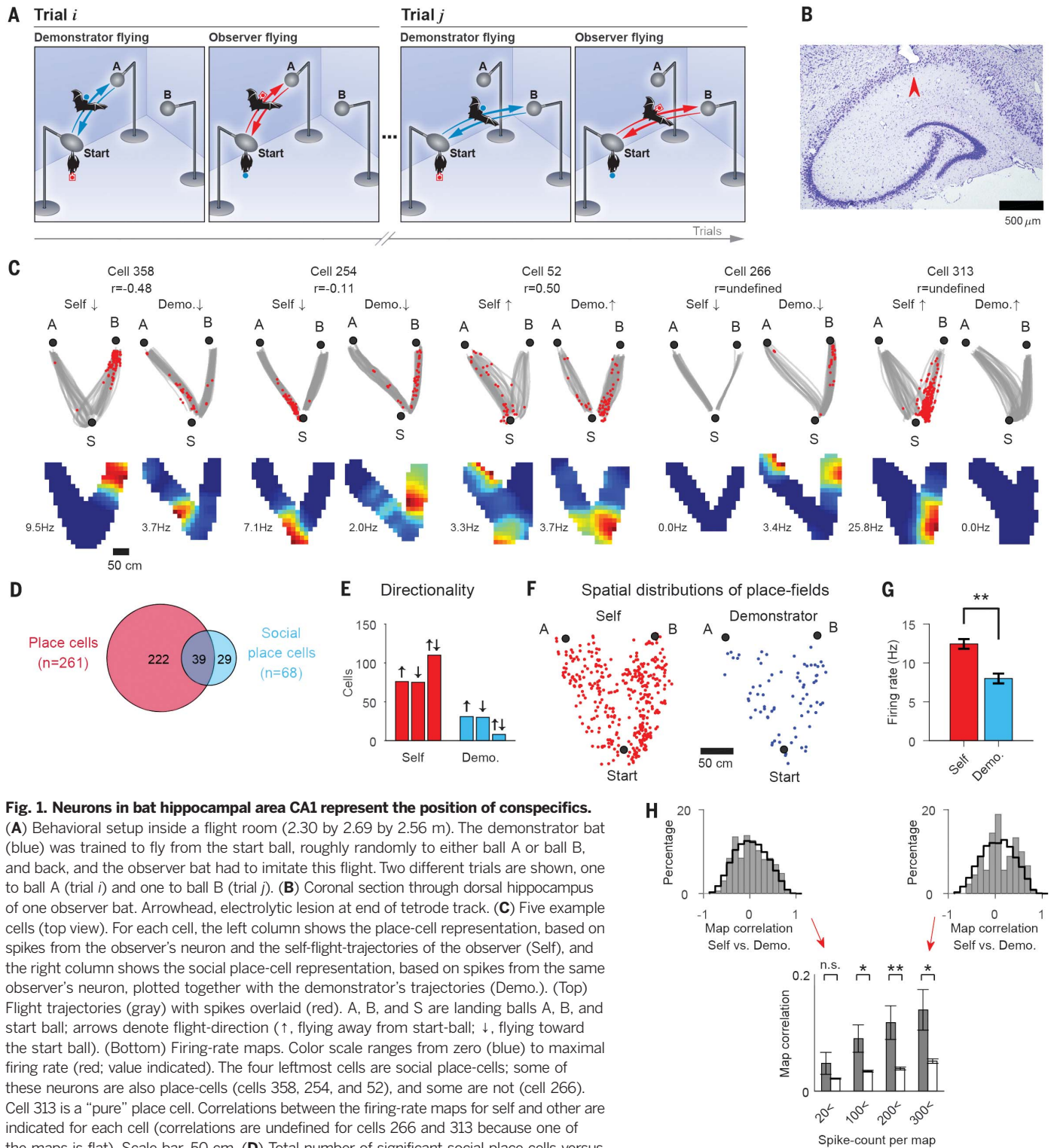


**Fig. 1. Neurons in bat hippocampal area CA1 represent the position of conspecifics.** (A) Behavioral setup inside a flight room (2.30 by 2.69 by 2.56 m). The demonstrator bat (blue) was trained to fly from the start ball, roughly randomly to either ball A or ball B, and back, and the observer bat had to imitate this flight. Two different trials are shown, one to ball A (trial *i*) and one to ball B (trial *j*). (B) Coronal section through dorsal hippocampus of one observer bat. Arrowhead, electrolytic lesion at end of tetrode track. (C) Five example cells (top view). For each cell, the left column shows the place-cell representation, based on spikes from the observer's neuron and the self-flight-trajectories of the observer (Self), and the right column shows the social place-cell representation, based on spikes from the same observer's neuron, plotted together with the demonstrator's trajectories (Demo.). (Top) Flight trajectories (gray) with spikes overlaid (red). A, B, and S are landing balls A, B, and start ball; arrows denote flight-direction (↑, flying away from start-ball; ↓, flying toward the start ball). (Bottom) Firing-rate maps. Color scale ranges from zero (blue) to maximal firing rate (red; value indicated). The four leftmost cells are social place-cells; some of these neurons are also place-cells (cells 358, 254, and 52), and some are not (cell 266). Cell 313 is a "pure" place cell. Correlations between the firing-rate maps for self and other are indicated for each cell (correlations are undefined for cells 266 and 313 because one of the maps is flat). Scale bar, 50 cm. (D) Total number of significant social place-cells versus significant classical place cells that we recorded. (E) Number of place cells and social place-cells that were significantly tuned to one flight-direction (↑), the other flight-direction (↓), or both directions (↑↓). Classical place cells are in red ( $n = 261$ ), and social place-cells are in blue ( $n = 68$ ). (F) Locations of peak firing for all the significant maps for place cells (red dots,  $n = 371$  cells × directions), and social place-cells (blue dots,  $n = 76$  cells × directions); cells that had significant tuning in both directions were depicted twice; hence, the counts here are larger than in (D). Dots were randomly jittered by up to ±5 cm (half bin) for display purposes. (G) Average peak firing rate for all the classical place cells (red,  $n = 371$  cells × directions) and all the social place-cells (blue,  $n = 76$  cells × directions).  $**P < 0.01$ . (H) (Top) Distributions of correlation coefficients between classical place cell maps and social place-cell maps for all the neurons that encoded significantly either self-position or conspecific position and had >20 spikes per map (left histogram) or >300 spikes per map (right histogram). Gray, the data; black lines, cell-shuffling distributions (14). (Bottom) Map correlations increased with firing rate. Error bars, mean ± SEM; gray bars, the data; open bars, cell-shuffling; number of cells × directions included in the four bars:  $n = 334, 218, 137, \text{ and } 91$ ;  $*P < 0.05$ ;  $**P < 0.01$ ; n.s., nonsignificant.

Downloaded from <http://science.sciencemag.org/> on January 25, 2018

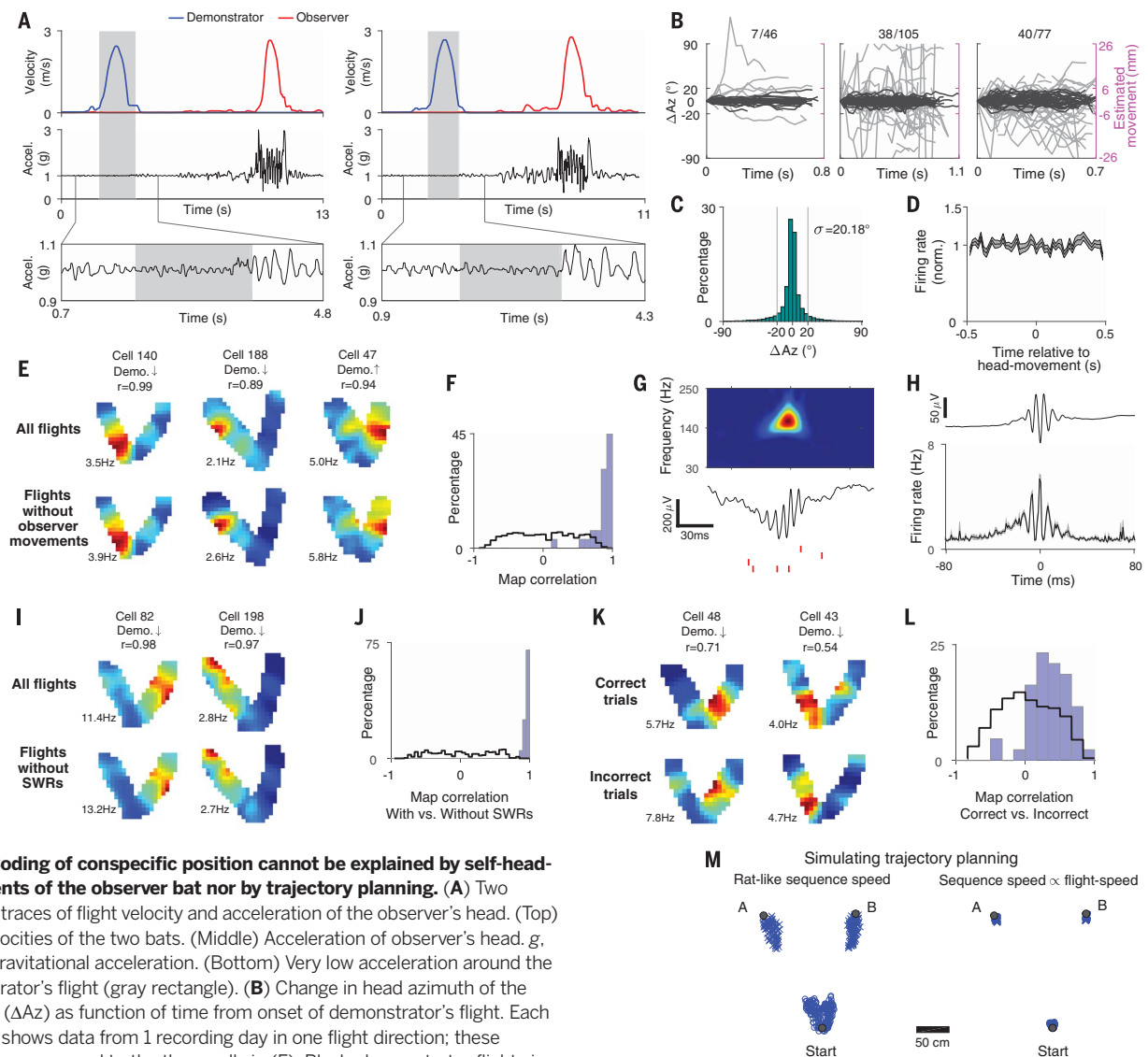


**Fig. 2. Coding of conspecific position cannot be explained by self-head-movements of the observer but nor by trajectory planning.** (A) Two example traces of flight velocity and acceleration of the observer’s head. (Top) Flight velocities of the two bats. (Middle) Acceleration of observer’s head. *g*, Earth’s gravitational acceleration. (Bottom) Very low acceleration around the demonstrator’s flight (gray rectangle). (B) Change in head azimuth of the observer ( $\Delta Az$ ) as function of time from onset of demonstrator’s flight. Each example shows data from 1 recording day in one flight direction; these examples correspond to the three cells in (E). Black, demonstrator flights in which the observer’s head moved  $<1$  SD ( $\sigma = 20.18^\circ$ , which corresponds to  $<6$  mm movement; right y axis) (14). Gray, demonstrator flights that included deviant head movements of the observer bat that exceeded  $\pm\sigma$ . Numbers indicate proportion of deviant flights out of all the flights on this day. (C) Distribution of  $\Delta Az$  of the observer’s head, pooled over all days with significant social place-cells where motion-sensor data were recorded ( $n = 18$  days,  $n = 35,284$  samples). Gray lines mark 1 SD ( $\sigma = 20.18^\circ$ ), which was the threshold used in (B) to define deviant flights. (D) Mean firing rate of social place-cells outside the task, triggered on the peak velocity of observer’s head movements, for all the 1-s segments with small angular displacement  $<20^\circ$  ( $n = 14,893$  segments, pooled over all significant social place-cells with motion-sensor data; shaded area indicates mean  $\pm$  SEM). (E) Three example cells, showing high correlation between social place field maps before (top) and after (bottom) removal of all the flights that included observer head-movements [At bottom, we removed all gray-colored flights in (B) and the corresponding spikes]. (F) Blue histogram, distribution of correlation coefficients between social place-cell maps with and without removal of flights with observer movements. Black line, cell-shuffling distribution. We included here all the significant social place-cells where motion-sensor data were recorded ( $n = 29$  cells  $\times$  directions). Shown are high correlations between maps with versus without removal of flights with observer movements (blue histogram); *t* test with unequal variances, compared with cell-shuffling control (black):  $P < 10^{-26}$ . (G) Example of a SWR. (Top) Spectrogram of the SWR. (Middle) Raw LFP trace (1 to 400 Hz bandpass). Scale bars, 30 ms and 200  $\mu V$ . (Bottom) Spikes from

four simultaneously recorded neurons (red ticks). Same time scale in all panels. (H) (Top) Mean SWR waveform, averaged across all recording days with social place-cells ( $n = 46$  days;  $n = 9,092$  SWRs). (Bottom) SWR-triggered firing rate, averaged over all neurons recorded during days with social place-cells ( $n = 276$  neurons; shaded area, mean  $\pm$  SEM). (I) Two social place-cells (columns), showing high stability with versus without flights that included SWRs (top versus bottom). (J) Distribution of correlation coefficients between social place-cell maps and the same maps after removal of flights with SWRs. Blue histogram, data for all cells with  $>20$  spikes per map that had SWRs during observer flights ( $n = 20$  cells  $\times$  directions). Black line, cell-shuffling distribution. *t* test with unequal variances, data compared with cell-shuffling control:  $P < 10^{-140}$ . (K) Two social place-cells (columns), showing high stability in correct trials (top) versus incorrect trials (bottom). (L) Distribution of correlation coefficients between social place-cell maps computed by using correct trials versus incorrect trials. Blue histogram, data for all neurons with  $>20$  spikes per map ( $n = 43$  cells  $\times$  directions). Black line, cell-shuffling distribution. *t* test with unequal variances, data compared with cell-shuffling control:  $P < 10^{-8}$ . We included in this analysis only cells with  $>15$  correct flights and  $>15$  incorrect flights;  $n = 43$  cells  $\times$  directions. (M) (Left) Simulated spatial distribution of social place fields, assuming that they are generated by place cell sequences with a ratlike sequence-speed of 8 m/s (14). (Right) Same, using a sequence speed of 43 m/s, which is scaled up to the flight speed of the demonstrator bat (corresponding to 20 times the bat’s flight speed in our task). Blue circles and crosses denote cells with preferred direction  $\uparrow$  and  $\downarrow$ , respectively.

maps, as indicated by very high map-correlations (Fig. 2, I, examples, and J, population), suggesting that social place fields are not created by SWR-associated trajectory planning. (ii) Next, we analyzed the neuronal activity during correct versus incorrect trials because studies in rats showed that hippocampal cell-assembly activity is strongly correlated to choice behavior on correct/incorrect trials (17). We reasoned that if the firing of the neurons reflects planning, then there would be a difference between social place-cell maps computed by using correct versus incorrect trials (where “incorrect” means that the demonstrator’s flight was followed by an incorrect flight of the observer)—because before incorrect flights, the observer bat is likely planning to fly to the opposite landing ball from the demonstrator. However, we found high correlations between correct-trial maps and incorrect-trial maps (Fig. 2, K, examples, and L, population). (iii) Trajectory planning has been linked to hippocampal place cell sequences (16), and such sequences might potentially create the social place fields that we observed. However, this seems highly unlikely because place cell sequences play extremely rapidly—at a speed of 8 m/s in rats (18), which is ~20 times faster than the running speed of the animal (18)—and therefore, all the firing of the observer’s neurons would be spatially compressed in one location, such as immediately after the takeoff of the demonstrator (14). Indeed, simulations of place-cell sequences confirmed this: All the place fields in this simulation were spatially compressed near the takeoff balls (Fig. 2M, blue crosses and circles), unlike the experimentally observed uniform distribution of social place fields (Fig. 1F, right). Together, this argues that social place fields cannot be explained via trajectory planning by the observer bat. Moreover, if trajectory planning in the observer’s brain is somehow synchronized precisely to the timing and velocity of each of the demonstrator’s flights—

which seems rather unlikely—then it constitutes an explicit spatial representation of the position of the other bat.

Classical place cells in CA1 represent the animal’s self-position in a world coordinate-frame: “allocentric coordinates” (1). To test whether social place-cells also form an allocentric representation, we exploited the fact that although the bats did not move their head much during the demonstrator flights (Fig. 2, A to C), the head did point in different azimuthal directions across different flights (we focused here on the azimuthal angle because the observer bats mainly moved their head in azimuth) (Fig. 3, A and B, and fig. S4) (14). For each of the social place-cells, we computed the median head azimuth of the observer (Fig. 3B, red line) and then used this median to divide all the demonstrator’s flights into two halves, corresponding to the observer bat looking right versus looking left (Fig. 3C, top versus bottom, respectively). If social place-cells are allocentric, then we expect similar maps irrespective of the head azimuth of the observer. Indeed, maps computed during right-viewing and left-viewing were rather similar (Fig. 3, C, examples, and D, population), which is consistent with an allocentric representation. Further, there was no relation between the map correlation and the average head direction difference between looking right and looking left [correlation coefficient ( $r$ ) = -0.12,  $P$  = 0.59; the head-direction differences spanned a broad range, from  $\Delta\text{Az}$  =  $30^\circ$  to  $102^\circ$ ] (Fig. 3E and fig. S4), which also is consistent with an allocentric representation. These neurons are thus fundamentally different from vectorial goal-direction cells in the bat hippocampus, which represent the direction to navigational goals in egocentric coordinates (19).

Last, we asked whether a flying conspecific is represented differently from inanimate moving objects. We conducted additional experiments in

two of the four recorded bats. These experiments included three sessions (Fig. 4A). Session 1 was conducted as before (Fig. 1A). In session 2, we moved an object either to ball A or to ball B, and the observer bat had to imitate it; it was the same task as before, but with an object instead of a conspecific. We termed this object an “informative object” (Fig. 4A, session 2, and fig. S5B) (14). In session 3, the observer bat was trained to hang at a fixed position on the start ball and to do nothing, while we moved a different object, a “noninformative object” (in this session, the observer bat did not receive reward and hence did not fly) (Fig. 4A, session 3, and fig. S5C). Both objects were similar in size to a flying bat (fig. S5). Surprisingly, we found quite a few CA1 cells that encoded the position of inanimate moving objects (Fig. 4, B, four top examples, and C, population); to our knowledge, this is the first report that the position of moving objects is explicitly represented in the hippocampus [a previous study reported modulation of place cell firing by the movement of another object, but not an explicit spatial representation of that object (20)]. Some of the CA1 cells represented both the inanimate objects and the conspecific (Fig. 4B, cells 184, 169, and 361); some cells represented only the objects (Fig. 4B, cell 182); and some cells represented only the conspecific (Fig. 4B, cell 221 and C, population summary). There were some differences between the representations of the conspecific and the inanimate objects. First, there was a slight trend for a better encoding of space (higher spatial information) going from the demonstrator bat to the informative object and to the noninformative object (Wilcoxon rank-sum tests, informative object versus noninformative object,  $P$  < 0.05; demonstrator bat versus noninformative-object,  $P$  = 0.093; demonstrator bat versus informative-object,  $P$  = 0.824; Kruskal-Wallis test,  $P$  = 0.092) (Fig. 4D). Second, whereas the representation of

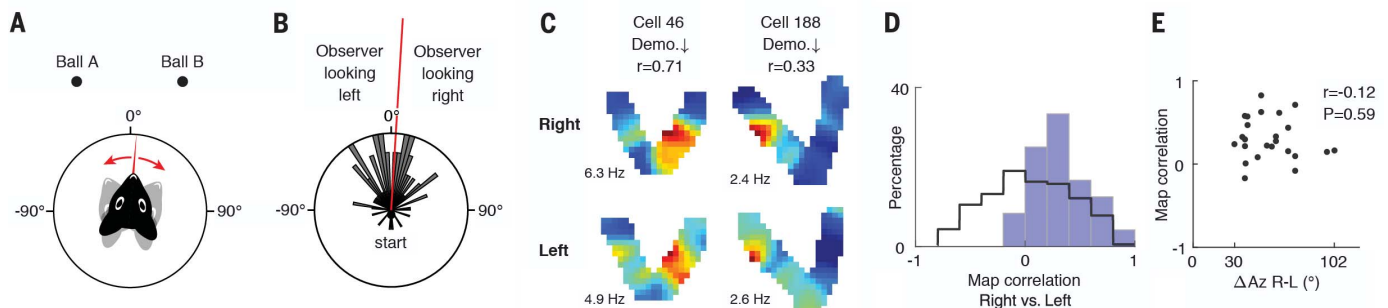


**Fig. 3. The representation of conspecifics is allocentric, not egocentric.**

(A and B) Dividing the demonstrator’s flight data based on the observer’s head direction during demonstrator’s flights. (A) Schematic drawing of directional notations of the bat’s head relative to the two landing balls. (B) Distribution of the azimuthal head directions of the observer during demonstrator flights; data from 1 recording day. The median head direction ( $6.8^\circ$ ) is plotted in red. Direction  $0^\circ$  is parallel to the east-west wall of the room. (C) Two cells showing stability of their social place fields between right-pointing head directions (top) and left-pointing head directions (bottom). (D) Blue histogram, distribution of the correlation coefficients between right-

looking maps and left-looking maps (blue), plotted for all the social place-cells for which we recorded motion-sensor data and had >20 spikes per map ( $n$  = 24 cells  $\times$  directions);  $t$  test with unequal variances, compared with cell-shuffling control (black):  $P$  <  $10^{-4}$ . Black line, cell-shuffling distribution, consisting of correlations between left-looking maps from cell  $i$  and right-looking maps from cell  $j$  across all the cell pairs where  $i \neq j$ . (E) Scatter plot of the similarity between right-looking and left-looking maps (y axis), versus the difference between the means of the right-looking and left-looking angles (x axis). No correlation was found ( $r$  = -0.12,  $P$  = 0.59; shown is a large span of azimuthal head-direction angles).

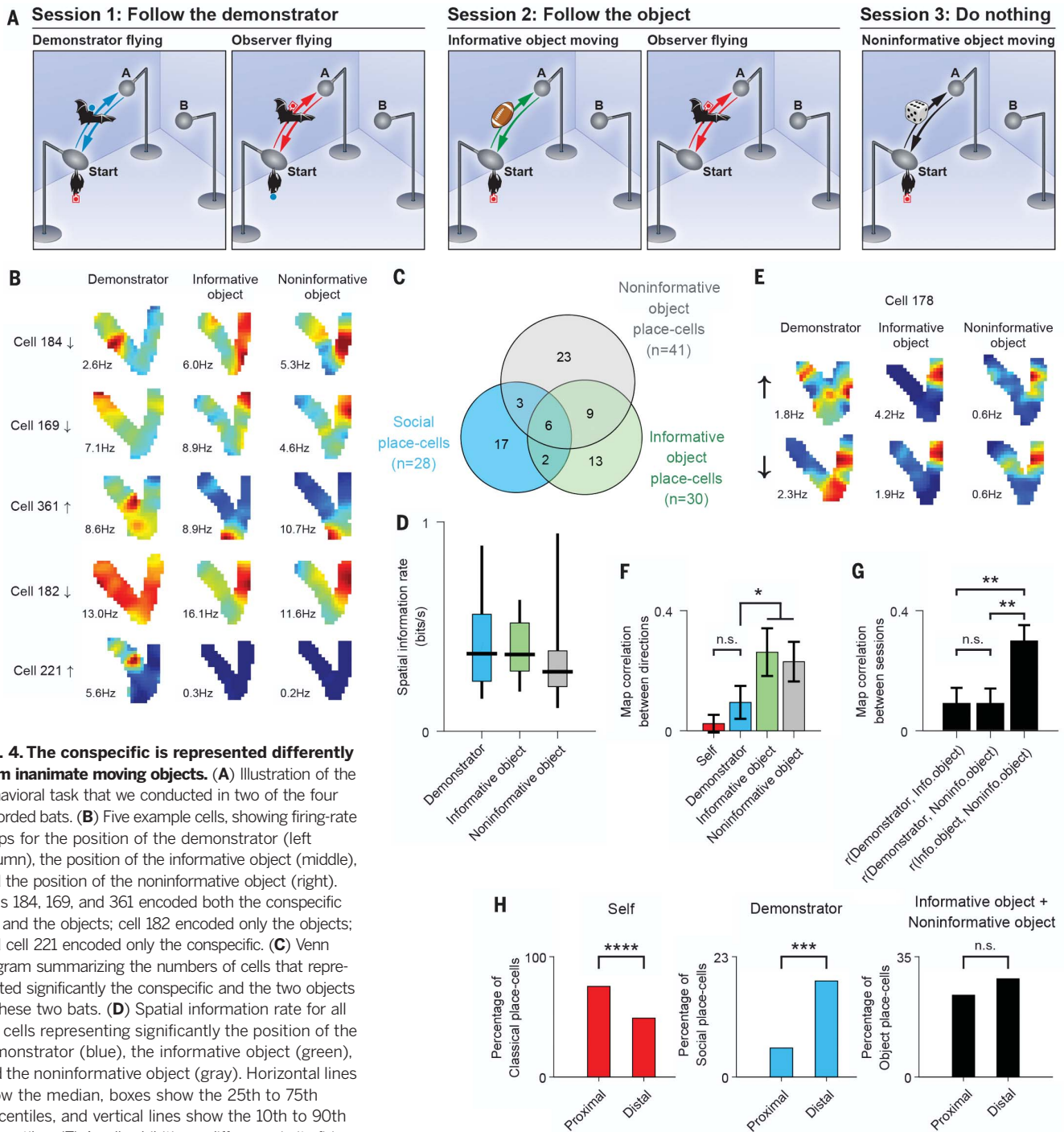


**Fig. 4. The conspecific is represented differently from inanimate moving objects.** (A) Illustration of the behavioral task that we conducted in two of the four recorded bats. (B) Five example cells, showing firing-rate maps for the position of the demonstrator (left column), the position of the informative object (middle), and the position of the noninformative object (right). Cells 184, 169, and 361 encoded both the conspecific bat and the objects; cell 182 encoded only the objects; and cell 221 encoded only the conspecific. (C) Venn diagram summarizing the numbers of cells that represented significantly the conspecific and the two objects in these two bats. (D) Spatial information rate for all the cells representing significantly the position of the demonstrator (blue), the informative object (green), and the noninformative object (gray). Horizontal lines show the median, boxes show the 25th to 75th percentiles, and vertical lines show the 10th to 90th percentiles. (E) A cell exhibiting a difference in its firing-rate maps between different flight directions of the demonstrator bat (left column), but showing no directionality for the two objects (middle and right columns); compare the top and bottom maps for the two objects (direction  $\uparrow$  vs  $\downarrow$ ). (F) Directionality: population summary. Shown are correlations of firing-rate maps between the two flight directions: for the self-representation, the demonstrator bat, and the informative and noninformative objects (data for all cells in which at least one flight direction exhibited a significant map, and both maps contained  $>50$  spikes per map). The maps are much more directional (lower correlations) for the demonstrator than for the two objects;  $t$  test for the correlations between the two directions for demonstrator-bat versus the two pooled objects:  $*P < 0.05$ . (G) Correlations of firing-rate maps for demonstrator bat versus informative object (left), demonstrator bat versus noninformative object (middle), and informative

object versus noninformative object (right). Correlations here were computed for all cells in which at least one of the two maps was significant, and only for maps with  $>50$  spikes;  $t$  test of the object-object similarity versus the conspecific-object similarities:  $**P < 0.01$  for both comparisons. To increase the robustness of comparisons between demonstrator and objects, (C), (D), (F), and (G) included only cells that met a strict criterion of  $>25$  flights per map and  $>50$  spikes per map. (H) Functional anatomy along the proximal-distal axis of CA1, for one of the two bats tested with three sessions (14). Shown is the percentage of significant tuning, separately for proximal and distal tetrodes. (Left) Place cells (Self). (Middle) Social place-cells (Demonstrator). (Right) Object place cells (pooled over both objects).  $***P < 10^{-3}$ ,  $****P < 10^{-5}$ .

the conspecific was directional—akin to the directionality exhibited by self place fields—the representation of both objects was nondirectional, that is, rather similar in both directions (Fig. 4, E, example, and F, population). Third, the representation of the demonstrator bat was significantly less similar to any of the object representations, as compared with the similarity between the two object representations (Fig. 4, B, cells 184,169, and 361; E, examples of similar firing for both objects; and G, population) (controls for spatial-coverage, velocity, and firing-rate are provided in fig. S6). Fourth, we found a significant difference in the functional-anatomical gradient between social place-cells and object place cells, along the proximodistal axis of CA1. Social place-cells were significantly more prevalent closer to the distal border of CA1 (log odds-ratio test:  $P < 10^{-3}$ ) (Fig. 4H, middle, and fig. S7) (14), unlike object place-cells, which did not exhibit a significant proximodistal gradient (log odds-ratio test:  $P = 0.17$ ) (Fig. 4H, right). Social place-cells exhibited the opposite pattern from classical place cells, which—consistent with previous reports in rats (21)—were significantly more prevalent near the proximal border of CA1 (log odds-ratio test:  $P < 10^{-5}$ ) (Fig. 4H, left). However, this result (Fig. 4H) was obtained from a single animal (out of the two bats tested in all three sessions), in which we had a sufficient number of neurons and good proximodistal span of tetrodes (14); future studies will need to examine this in more detail. Together, these results suggest that the representation of the conspecific is rather different from the representation of inanimate objects, indicating that the spatial coding of the conspecific is not a simple sensory response driven by any sensory stimulus that moves through the social place field. Rather, these are context-dependent cognitive representations.

We found in this work a subpopulation of cells in bat dorsal CA1 that encode the position of conspecifics, in allocentric coordinates. This representation could not be explained by self-head-movements or by self-trajectory-planning. The responses to the conspecific were directional, which is in line with the directionality of classical place cells, but can also be interpreted through the social difference between an approaching and receding conspecific. Social place fields are unlikely to reflect either distance-coding (observer-demonstrator distance) or time-coding (time since demonstrator-takeoff) because in both cases, we would expect rather symmetric firing fields on flights to both ball A and ball B, whereas nearly all the social place-cells had a firing field on one side only. However, an alternative interpretation is that these neurons encode a position-by-time signal: Namely, they encode the spatial side to which the demonstrator bat is flying, together with its time from takeoff. We also found qualitative differences between the spatial representations of conspecifics versus inanimate moving objects. The different encoding of conspecifics versus objects may arise from (partially) dif-

ferent mechanisms. For example, spatial representation of moving objects in CA1 might arise from convergence of spatial inputs from grid cells in the medial entorhinal cortex (4, 6) and object-related inputs from neurons in the lateral entorhinal cortex (22, 23); by contrast, social place-cells may also involve socially modulated inputs from CA2 (24, 25). Future studies are thus needed in order to search for social place-cells in the bat CA2, medial, and lateral entorhinal cortices, as well as in the ventral CA1, which was recently shown to be important for social memory (26).

It may seem surprising that social place-cells were not discovered previously in several studies of rat hippocampus that looked for a modulation of classical place fields by the presence of conspecifics (27–29). We believe that the key difference is in the task: In those previous studies, there was no incentive for the animal to pay attention to the position of the conspecific; our task, in contrast, required the bat to pay close attention to the position of the other bat and to hold this position in memory during a 12.7-s average delay, which revealed a spatial representation for the other. This interpretation is consistent with many studies that showed that hippocampal representations are highly task-dependent, plastic, and memory-dependent (30–32). Additionally, this task created a high level of social interactions between the two bats: When the bats were together at the start ball, they often approached and touched each other and emitted many social vocalizations (fig. S8), and this intensely social situation may have contributed to the representation of the conspecific.

There is an apparent similarity between the social place-cells, which encode the position of the other, and “mirror neurons” in monkeys, which encode the actions of the other (33). One difference, however, is that noncongruent social place-cells (Fig. 1C, cells 358 and 254) are still useful functionally because they encode meaningful information about the position of the other, whereas it is less clear how noncongruent mirror neurons in monkeys might be useful for the proposed functions of mirror neurons. Thus, social place-cells are conceptually different from mirror neurons, although both might possibly share a similar functional principle, whereby the same neuronal circuit can be used for self-representation as well as for representing conspecifics.

Last, we speculate that social place-cells may play a role in a wide range of social behaviors in many species—from group navigation and coordinated hunting to observational learning, social hierarchy, and courtship—and may be relevant also for the representation of nonconspecific animals—for example, for spatial encoding of predators and prey. These results open many questions for future studies: How are multiple animals represented in the brain? Is there a different representation for socially dominant versus subordinate animals, and for males versus females? These and many other questions await investigation in or-

der to elucidate the neural basis of social-spatial cognition.

## REFERENCES AND NOTES

1. J. O'Keefe, L. Nadel, *The Hippocampus as a Cognitive Map* (Oxford Univ. Press, 1978).
2. M. A. Wilson, B. L. McNaughton, *Science* **261**, 1055–1058 (1993).
3. N. Ulanovsky, C. F. Moss, *Nat. Neurosci.* **10**, 224–233 (2007).
4. T. Hafting, M. Fyhn, S. Molden, M.-B. Moser, E. I. Moser, *Nature* **436**, 801–806 (2005).
5. C. Barry, R. Hayman, N. Burgess, K. J. Jeffery, *Nat. Neurosci.* **10**, 682–684 (2007).
6. M. M. Yartsev, M. P. Witter, N. Ulanovsky, *Nature* **479**, 103–107 (2011).
7. J. S. Taube, R. U. Muller, J. B. Ranck Jr., *J. Neurosci.* **10**, 420–435 (1990).
8. A. Peyrache, M. M. Lacroix, P. C. Petersen, G. Buzsáki, *Nat. Neurosci.* **18**, 569–575 (2015).
9. A. Finkelstein et al., *Nature* **517**, 159–164 (2015).
10. T. Solstad, C. N. Boccara, E. Kropff, M.-B. Moser, E. I. Moser, *Science* **322**, 1865–1868 (2008).
11. F. Savelli, D. Yoganarasimha, J. J. Knierim, *Hippocampus* **18**, 1270–1282 (2008).
12. C. Lever, S. Burton, A. Jeewajee, J. O'Keefe, N. Burgess, *J. Neurosci.* **29**, 9771–9777 (2009).
13. G. Neuweiler, *The Biology of Bats* (Oxford Univ. Press, 2000).
14. Materials and methods are available as supplementary materials.
15. M. M. Yartsev, N. Ulanovsky, *Science* **340**, 367–372 (2013).
16. B. E. Pfeiffer, D. J. Foster, *Science* **349**, 180–183 (2015).
17. J. Ferbinteanu, M. L. Shapiro, *Neuron* **40**, 1227–1239 (2003).
18. T. J. Davidson, F. Kloosterman, M. A. Wilson, *Neuron* **63**, 497–507 (2009).
19. A. Sarel, A. Finkelstein, L. Las, N. Ulanovsky, *Science* **355**, 176–180 (2017).
20. S. A. Ho et al., *Neuroscience* **157**, 254–270 (2008).
21. E. J. Henriksen et al., *Neuron* **68**, 127–137 (2010).
22. A. Tsao, M.-B. Moser, E. I. Moser, *Curr. Biol.* **23**, 399–405 (2013).
23. J. J. Knierim, J. P. Neunuebel, S. S. Deshmukh, *Philos. Trans. R. Soc. Lond. B Biol. Sci.* **369**, 20130369 (2013).
24. F. L. Hitti, S. A. Siegelbaum, *Nature* **508**, 88–92 (2014).
25. S. M. Dudek, G. M. Alexander, S. Farris, *Nat. Rev. Neurosci.* **17**, 89–102 (2016).
26. T. Okuyama, T. Kitamura, D. S. Roy, S. Itoharu, S. Tnegawa, *Science* **353**, 1536–1541 (2016).
27. L. Zinyuk, J. Huxter, R. U. Muller, S. E. Fox, *Hippocampus* **22**, 1405–1416 (2012).
28. M. von Heimendahl, R. P. Rao, M. Brecht, *J. Neurosci.* **32**, 2129–2141 (2012).
29. X. Mou, D. Ji, *eLife* **5**, e18022 (2016).
30. E. J. Markus et al., *J. Neurosci.* **15**, 7079–7094 (1995).
31. M. A. Moita, S. Rosis, Y. Zhou, J. E. LeDoux, H. T. Blair, *Neuron* **37**, 485–497 (2003).
32. H. Eichenbaum, N. J. Cohen, *Neuron* **83**, 764–770 (2014).
33. G. Rizzolatti, C. Sinigaglia, *Nat. Rev. Neurosci.* **17**, 757–765 (2016).

## ACKNOWLEDGMENTS

We thank K. Haroush, S. Romani, O. Forkosh, A. Rubin, M. Geva-Sagiv, A. Finkelstein, T. Eliav, G. Ginosar, A. Sarel, and D. Blum for comments on the manuscript; S. Kaufman, O. Gobi, and S. Futerman for bat training; A. Tuval for veterinary support; C. Ra'anan and R. Eilam for histology; B. Pasmantir and G. Ankaoua for mechanical designs; and G. Brodsky for graphics. This study was supported by research grants to N.U. from the European Research Council (ERC-CoG-NATURAL\_BAT\_NAV), Israel Science Foundation (ISF 1319/13), and Minerva Foundation. The data are archived on the Weizmann Institute of Science servers and will be made available on request.

## SUPPLEMENTARY MATERIALS

www.sciencemag.org/content/359/6372/218/suppl/DC1  
Materials and Methods  
Figs. S1 to S8  
References (34–42)  
Movies S1 and S2

11 July 2017; accepted 7 December 2017  
10.1126/science.aao3474



## Supplementary Material for **Social place-cells in the bat hippocampus**

David B. Omer, Shir R. Maimon, Liora Las,\* Nachum Ulanovsky\*

\*Corresponding author. Email: nachum.ulanovsky@weizmann.ac.il (N.U.);  
liora.las@weizmann.ac.il (L.L.)

Published 12 January 2018, *Science* **359**, 218 (2017)  
DOI: 10.1126/science.aao3474

**This PDF file includes:**

Materials and Methods  
Figs. S1 to S8  
References

**Other Supplementary Material for this manuscript includes the following:**  
(available at [www.sciencemag.org/content/359/6372/218/suppl/DC1](http://www.sciencemag.org/content/359/6372/218/suppl/DC1))

Movies S1 and S2

## Materials and Methods

### Subjects and behavioral setup

Four pairs of adult male Egyptian fruit bats, *Rousettus aegyptiacus*, were included in this study (8 bats in total; weights 160–179 gr). Each pair consisted of an ‘observer bat’ and a ‘demonstrator bat’, which were trained to fly in a flight-room ( $2.30 \times 2.69 \times 2.56$  m). The room was dimly illuminated (illuminance level: 3 lux). Three landing-balls were positioned inside the room (the balls were denoted as ‘Start’, ‘A’ and ‘B’: see Fig. 1A, fig. S1A, and movie S1). Landing-balls A and B were elevated spheres (12-cm diameter, height above floor: 115 cm), positioned at the far corners of one side of the room; the start-ball was an elevated ellipsoid ( $12 \times 30$  cm, height above floor: 150 cm), positioned next to the wall that was opposite to balls A and B (Fig. 1A, fig. S1A). The linear distance between the start-ball and landing-balls A and B was ~170 cm. All behavioral sessions were performed in the same flight-room and same setup, without moving any of the balls. The demonstrator bat in each pair was usually the more dominant male, and it was a highly-trained animal – both of which played an important role in the task (see below). The observer bat in each pair was always the bat that, after training, was implanted with a microdrive for electrophysiological recordings (see below). The bats exhibited intense social interactions during the task when they were together on the start-ball – including approaching each other, touching, and producing many social vocalizations (fig. S8).

Each experimental day started with a sleep session and ended with a sleep session (each sleep session lasting at least 5 min). For the sleep session, the observer bat was placed alone inside a small cage which was positioned in the middle of the experimental flight-room, on the floor. The demonstrator bat was outside the room during sleep sessions.

In-between the two sleep sessions, we conducted three kinds of behavioral sessions. Session no. 1 – the “observer-demonstrator” session – was conducted in all 4 pairs of bats. We trained each pair of bats on a complementary set of rules: The demonstrator bat was trained to fly roughly randomly to ball A or to ball B, and then fly back to the start ball. The observer bat was trained to be stationary and wait for the demonstrator to return to the start ball, and after his return he had to imitate the demonstrator’s flight – i.e. the observer-bat had to fly to the same ball as the demonstrator-bat (Fig. 1A, and movies S1 and S2). The average delay between demonstrator-landing and observer-takeoff was  $12.7 \pm 8.6$  s (mean  $\pm$  s.d.). Bats were food-rewarded for correct performance by giving ~0.05 ml of banana mash on each correct trial. On average, each bat performed  $88 \pm 29$  back-and-forth flights in this session (mean  $\pm$  s.d.). The mean flight-duration (one way) of the observer bat and of the demonstrator bat in this task was 0.98 s and 0.84 s, respectively. The mean flight speeds for the observer and demonstrator were rather similar – 2.56 m/s and 2.69 m/s. At the end of the first session, the demonstrator bat was taken out of the flight room.

Note that this task had two key features: first, it required the observer to pay close attention to the demonstrator’s position, and to hold this position in memory during the delay period; and second, because the observer was stationary during the demonstrator’s flight, it allowed temporal dissociation of the effects of self-flights from the flights of the other bat (see more below).

We note that to get good performance in this task, we found that it was helpful to choose a pair of bats that had a clear hierarchy between them – such that, in each pair, the demonstrator bat was the more dominant male and the observer bat was a more subordinate male. This relationship between the bats was evident also outside the experiments, during feeding and other

behaviors in their shared housing. The non-symmetric hierarchy helped the behavioral shaping, by preventing direct competition over food. This facilitated our task by preventing the observer from flying out together with the dominant demonstrator – so the observer remained stationary while the demonstrator was flying, which was crucial for our “delayed match-to-place” task. Conversely, the dominant demonstrator did not fly out together with the subordinate observer because of two reasons: first, right after receiving a reward the demonstrator was less motivated to fly out. Second, the demonstrator was a highly-trained bat chosen for its high performance.

The observer-bat could track the position of the demonstrator-bat either using vision – as these bats see very well under the 3-lux illumination used here, or using echolocation – and indeed our dual-microphone ultrasonic recordings (see below) revealed that both bats emitted sonar clicks as the demonstrator was flying: The demonstrator emitted sonar clicks in order to navigate, while the observer emitted sonar clicks most likely in order to track the demonstrator. We did not attempt to control for which sensory system was used by the observer to track the demonstrator – and it likely used a combination of vision and echolocation.

Sessions no. 2 and 3 were conducted in 2 of the 4 pairs of bats (Fig. 4A). In session 2 – the “informative-object” session – the demonstrator bat was replaced by a plastic object (fig. S5B). The observer was trained to follow the same set of training rules as in the “observer-demonstrator” session, but this time it was trained to imitate the informative-object instead of the demonstrator-bat. The object was mounted on a thin metal rod and was manually moved from the start ball to either ball A or ball B, and then back. The target ball in each trial was changed roughly randomly. On average, the informative object was moved  $48 \pm 20$  back-and-forth trajectories in this session (mean  $\pm$  s.d.).

In the third session – the “noninformative object” session – we replaced the plastic object with a different plastic object (fig. S5C). In this session the observer was trained to hang from the start ball and do nothing, while the “noninformative” object was moved between the start ball and either ball A or B. The observer bat did not receive a reward in this session, and hence did not fly. On average, the noninformative object was moved  $98 \pm 26$  back-and-forth trajectories in this session (mean  $\pm$  s.d.).

The sessions were carried out in a fixed sequential order (Fig. 4A): sleep session  $\rightarrow$  observer-demonstrator session (session 1)  $\rightarrow$  informative-object session (session 2)  $\rightarrow$  noninformative-object session (session 3)  $\rightarrow$  sleep session. Neuronal activity was recorded continuously throughout all the sessions, including the sleep sessions, to assess the stability of the recorded neurons.

The experimenter was standing at a fixed position in the flight room – same position in all three sessions. Both plastic objects were mounted on a metal pole (length: 1.3 m, thickness: 1 cm), and were moved manually by the experimenter between the landing balls.

All experimental procedures were approved by the Institutional Animal Care and Use Committee of the Weizmann Institute of Science.

### **Surgery and recording techniques**

After the training of a bat-pair was completed, the observer bat was implanted with a four-tetrode microdrive (weight 2.1 gr), loaded with four tetrodes, where each tetrode was constructed from four strands of insulated wire (17.8  $\mu$ m diameter platinum-iridium wire) – as described previously (6, 9, 15, 19). Tetrodes were gold-plated to reduce wire impedance to the range between 0.3–0.7 M $\Omega$  (at 1 kHz). The microdrive was implanted above the right dorsal

hippocampus (3.1–3.5 mm lateral to the midline and 5.8–6.3 mm anterior to the transverse sinus that runs between the posterior part of the cortex and the cerebellum). Surgical procedures were similar to those described previously (6, 9, 15, 19, 34): We used an injectable anesthesia cocktail composed of Medetomidine 0.25 mg/kg, Midazolam 2.5 mg/kg and Fentanyl 0.025 mg/kg – and subsequently added additional injections as needed, based on monitoring the bat’s breathing and heart-rate. Following surgery, the tetrodes were slowly lowered towards the CA1 pyramidal cell layer; positioning of tetrodes in the layer was provisionally assessed by the presence of high-frequency field oscillations (‘ripples’) and associated neuronal firing, and was later verified histologically (e.g., Fig. 1B). For each bat, one tetrode was left in an electrically-quiet zone and served as a reference, and the remaining three tetrodes served as recording probes. During recordings, a 16-channel wireless neural-recording device (‘neural-logger’) was attached to an Omnetics connector on the microdrive. Signals from all 16 channels of the 4 tetrodes were amplified ( $\times 200$ ) and bandpass filtered (1 – 7,000 Hz), and were then sampled continuously at 29.3 kHz per channel, and stored on-board the neural-logger. During subsequent processing, the neural recording was further filtered between 600 – 6,000 Hz for spikes, and then 1-ms spike waveforms were extracted using a voltage threshold; additionally, we filtered the recorded neural data between 1 – 400 Hz to extract local-field-potentials (LFP).

### **Spike sorting**

All spike-sorting procedures were identical to those described previously (3, 6). Briefly, spike waveforms were sorted on the basis of their relative energies and amplitudes on different channels of each tetrode. Data from all sessions – the behavioral sessions and the two sleep sessions – were spike-sorted together. Well-isolated clusters of spikes were manually selected,

and a refractory period ( $<2$  ms) in the interspike-interval histogram was verified. We included only neurons that (i) were stably isolated throughout all the sessions, including the first and last sleep session; (ii) emitted more than 20 spikes in-flight in one of the directions, in at least one of the behavioral sessions. A total of 378 well-isolated, stable active cells were recorded from hippocampal area CA1 of four observer bats.

### **Video tracking, estimating the positions of the bats and the objects, and audio recordings**

The positions of the two bats (demonstrator and observer) were tracked simultaneously using two color cameras located at two of the upper corners of the room. The cameras were connected to a video-tracker system, which tracked the position of bright omnidirectional light-emitting diodes (LEDs) which were mounted on the bat's head. The two bats were tracked separately by the colors of the LEDs: red LED on the observer bat, and blue LED on the demonstrator bat (movie S2). We used different colors for tracking the objects in the two object-sessions: in the informative-object session, we placed a green LED on the object; and in the noninformative-object session, we placed a pair of blue and red LEDs on the noninformative object.

The video data were sampled at a 25-Hz rate. The 3D positions of the bats and objects were reconstructed using the direct linear transform algorithm applied on data from both cameras (15). We removed from the analysis a small number of recording days in which the video-based position tracking has malfunctioned.

Ultrasonic audio recordings of bat vocalizations (fig. S8) were performed in 2 of the 4 pairs of bats (same bats as in Fig. 4), using two ultrasonic microphones that were placed under the start-ball and between landing-balls A and B. The sounds were digitized at a sampling-rate of 150 kHz.

Analyses of all the behavioral and neural data in this study were done using custom code written in Matlab.

### **Estimating the head-azimuth of the observer**

We measured the 3D head-direction of the observer using a 9-axis motion sensor that was mounted on the observer's head, as part of the neural-logger. This motion-sensor includes a 3-axis accelerometer – which allows measuring the head-angle relative to the Earth's gravity-field, and a 3-axis magnetometer – which allows measuring the head-angle relative to the Earth's magnetic-field. Measuring the head-direction relative to these two geophysical axes of the Earth (gravity, magnetic field) allows to estimate the 3D head-direction, using standard techniques (35, 36).

In Figs 2 and 3 we focused on analyzing head-direction azimuth, because the observer-bats mainly moved their head in azimuth (fig. S4) – and because the behavior of the demonstrator-bats was confined mostly to the horizontal plane (fig. S1).

### **Extracting flights, and computing firing-rate maps**

Firing-rate maps were constructed for flight periods only – separately for the two flight directions: i.e. one map for the flights from the start-ball to landing-balls A,B ( $\uparrow$ ), and a separate map for the flights back ( $\downarrow$ ). Individual flights were identified by local peaks in the flight velocity that had maximal-velocity  $> 1.2$  m/s. Each flight was then correlated with the average flight velocity profile: Flights with Pearson correlation of  $r > 0.8$  were retained for analysis. To improve the accuracy in estimating flight velocity, the bat's position was smoothed using a smoothing spline (*csaps.m* in Matlab), based on which the instantaneous velocity was computed.

Further, to ensure that takeoff and landing data did not contaminate the flight epochs, we removed from analysis the parts of the flight-trajectory that were in the vicinity of the landing balls (~20 cm radius around each landing ball). Flight epochs were classified automatically as described above, and subsequently all flights were inspected in order to ensure that only directed flight-trajectories were included in the data-set (e.g. we manually removed the few flights where the bat flew to the wall). Overall, we excluded 8.4% of the flights which either had Pearson correlation of  $r \leq 0.8$  or were non-directed to the balls.

The bats' behavior was mostly restricted to a 2D horizontal slab around the height of the balls (fig. S1). Therefore, all the analyses and statistical tests in this study were performed strictly on the basis of 2D firing-rate maps (horizontal  $xy$  projection). For each neuron, we computed two maps separately for the two flight-directions (i.e. separately when flying away from the start-ball or towards the start-ball; see examples in fig. S3). To compute 2D classical place-cell firing-rate maps, we used spikes recorded from neurons in the observer's CA1 and the corresponding flight-trajectories of the observer. To compute 2D social firing-rate maps, we used spikes recorded from the observer's CA1 and the corresponding flight-trajectories of the *demonstrator*. We used fixed-sized spatial bins ( $10 \times 10 \text{ cm}^2$ ) and collapsed the time-spent (occupancy) data and the spike counts onto the horizontal 2D dimension ( $xy$ ). We smoothed both the spike-count and time-spent 2D maps with a fixed Gaussian kernel ( $\sigma = 1.5$  bins), and then divided, bin by bin, the smoothed 2D spike-count by the smoothed 2D time-spent. Spatial bins (2D pixels) in which the bat spent  $< 100$  ms during the session were excluded from analysis and from the 2D firing-rate map, and were colored white.

For all the firing-rate maps, the color-scale ranged from zero (blue) to maximal firing-rate (red) – except in cases when 2 maps (or more) were shown for the same neuron, and one of the

maps had  $< 20$  spikes: In such cases, all the maps were scaled to the maximal firing-rate across the maps (this occurred in Fig. 4B, cell 221; fig. S3A, cell 365; and fig. S3B, cells 52 and 123).

### **Quantifying spatial coding, definitions of place-cells and social place-cells, and map correlations**

Cells in our setup can show two different ways of encoding spatial information. One way is to encode a specific focal position along the flight trajectories. Another way is to code for a particular side of the flight trajectories with different firing rates (i.e. different firing-rates for flight-trajectories to ball A versus ball B). Therefore, we used here two different measures to capture spatial coding by the neurons (these measures were computed separately for the two flight-directions):

(i) We calculated a spatial information rate index (in bits per second) from the smoothed firing-rate maps, as:

$$\text{spatial information rate index} = \sum_i p_i \lambda_i \log_2 \frac{\lambda_i}{\lambda}$$

Where  $\lambda_i$  is the mean firing rate of the neuron in the  $i$ -th spatial bin,  $\lambda$  is the overall mean firing rate, and  $p_i$  is the probability of the animal being in the  $i$ -th bin (occupancy in the  $i$ -th bin / total recording time) (37).

(ii) We calculated a side-coding index, as:

$$\text{side coding index} = \frac{\text{abs}(r_A - r_B)}{r_A + r_B}$$

Where  $r_A$  is the mean firing-rate in flight trajectories to or from ball A, and  $r_B$  is the mean firing-rate in flight trajectories to or from ball B (with the mean rate computed as the total number of

spikes on each side, divided by the total time spent in-flight on that side and in that flight-direction).

We used a shuffling procedure to determine if a recorded neuron was a place-cell or a social place-cell – by comparing the empirical value of the spatial information rate index for each cell to a spike-shuffled distribution; and similarly for the side-coding index. The same shuffling was used for both indices. The shuffled distribution was generated by randomly shifting the timestamps of the cell’s spike-train circularly within each flight (random circular spike-train shift), and then randomly reassigning the spike-trains to flights (random permutation of flights – which also resulted in randomizing the side [A or B] to which the spikes belonged). This shuffling procedure was repeated 1,000 times for each neuron – separately for the two flight directions ( $\uparrow$  or  $\downarrow$ ). For each repetition, the 2D firing-rate maps were generated anew in the same manner as described above, and the spatial information rate and side-coding index were recomputed. Active neurons for which the empirical values of the spatial information rate or of the side-coding index exceeded the upper 95% confidence interval of their shuffled distributions, for at least one of the two flight directions ( $\uparrow$  or  $\downarrow$ ), were defined as significant place-cells – if they were significant for the classical place-cell map (based on self-flights); or as significant social place-cells – if they were significant for the social place-cells map (based on demonstrator-flights). We similarly defined significant maps for the informative object and noninformative object.

Pearson correlations between firing-rate maps (‘map correlations’) were computed for pairs of maps which included  $> 20$  spikes per map. We compared all the histograms of map-correlations (Figs 1H, 2F, 2J, 2L and 3D) to cell-shuffling distributions (control distributions),

which comprised of all the map-correlations between a map from cell  $i$  and a map from cell  $j$  where  $i \neq j$  (i.e. map-correlations for all the non-identical cell-pairs).

To allow robust comparisons of the tuning properties of demonstrator-bat maps versus informative-object maps and noninformative-object maps (Fig. 4C, D, F, G; and fig. S6), we included in these population analyses only maps that were based on >25 flights per map and >50 spikes per map.

### **Detection of sharp-wave ripples and removal of neuronal firing around ripples**

To detect sharp-wave ripple (SWR) events, the LFP signal was filtered between 100–200 Hz and the instantaneous power of the signal was computed using the Hilbert transform. SWR events were defined by using two criteria. First, we extracted events in which the power of the bandpass-filtered LFP (100–200 Hz) exceeded a threshold of 3 s.d. above the mean. Second, we used a ‘ripple/high-gamma ratio’ – the ratio between the peak power of the LFP signal between 100–200 Hz (ripple range), and the peak power of the LFP between 60–100 Hz (high gamma range) – and required a ratio of  $> 1.5$  in order to discern clear spectral peaks in the ripple range. Only candidate SWR events which met both criteria – i.e. power  $>$  mean + 3 s.d., and ripple/high-gamma ratio  $> 1.5$  – were selected for further analysis. The average SWR rate was 0.060 Hz during sleep, and 0.051 Hz during the behavioral epochs when the observer-bat was stationary on the start-ball and the demonstrator-bat was flying.

In rats, a large majority of place-cell sequences occur during SWR events (38-42). To assess the possible contribution of SWR events to the social place-cells firing maps, we recalculated the firing maps by using only ripple-free flights, and compared them to social place-cell maps calculated using all flights (Fig. 2I-J). We included in this analysis only maps with

>20 spikes per map, in which SWRs occurred in the observer's CA1 during > 5% of the demonstrator's flights.

### **Simulating trajectory-planning via place-cell sequences**

In Fig. 2M-left, we tested an alternative potential explanation – that social-place-fields might reflect trajectory-planning by the observer-bat. Trajectory-planning in rats has been linked to hippocampal place-cell sequences (16), and such sequences might potentially create the social place-fields that we observed. To test this, we conducted simulations assuming that the firing of the neuron reflects self-place-cell sequences that begin exactly at the moment of the takeoff of the demonstrator-bat, and play at a typical speed reported for place-cell sequences in rats – namely 8 m/s (18). The distance of the self-place-field from the takeoff ball was linearly compressed proportionally to the ratio between the rat-like sequence-speed of 8 m/s and the average flight-speed of the demonstrator bat (2.14 m/s) – a compression ratio of 3.74. In Fig. 2M-right, we conducted a similar simulation, but here we assumed not a rat-like sequence-speed, but a rat-like compression-ratio – a compression ratio of 20, as reported previously in rats (18), and thus self-place-cell sequences played at a speed of 43 m/s ( $20 \times 2.14$  m/s). The fast sequence-speeds meant that the neurons' firing should occur within a very short time after takeoff – corresponding to a very short distance (of the demonstrator) from the takeoff-point. Indeed, in both simulations, the place-field locations (blue crosses or circles) have shrunk towards the takeoff-point of the demonstrator, i.e. close to the start-ball or to balls A, B (here we included all the place-cells – with directionality both towards and away from the start-ball – and hence place-fields could occur near any of the balls).

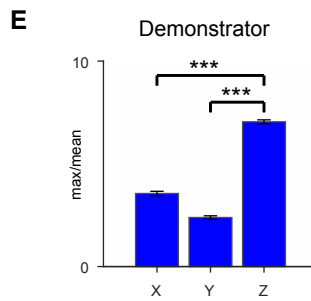
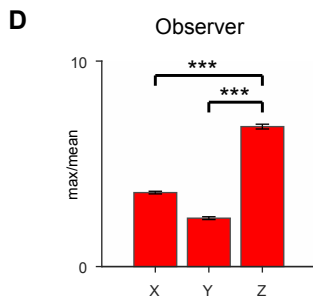
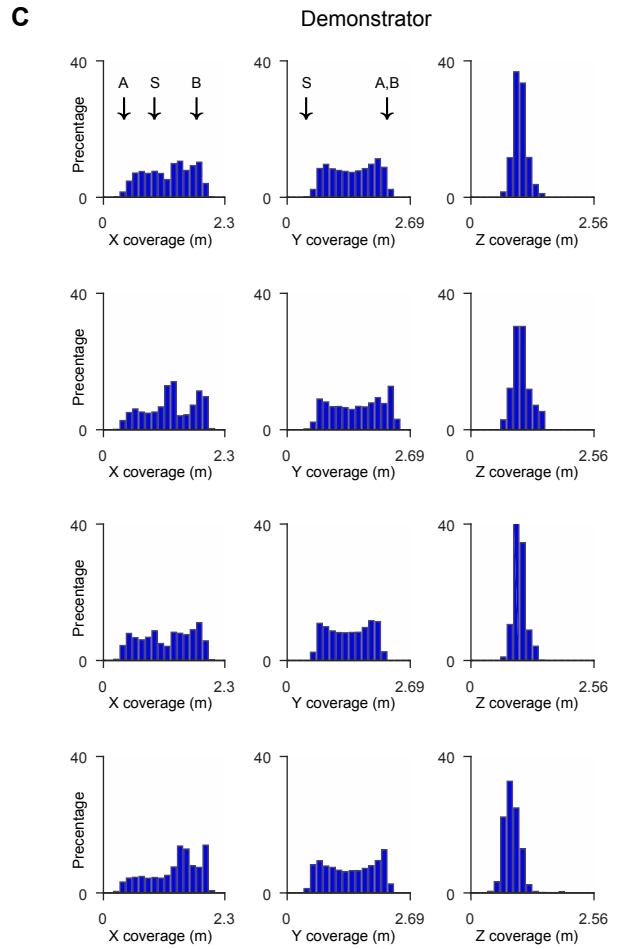
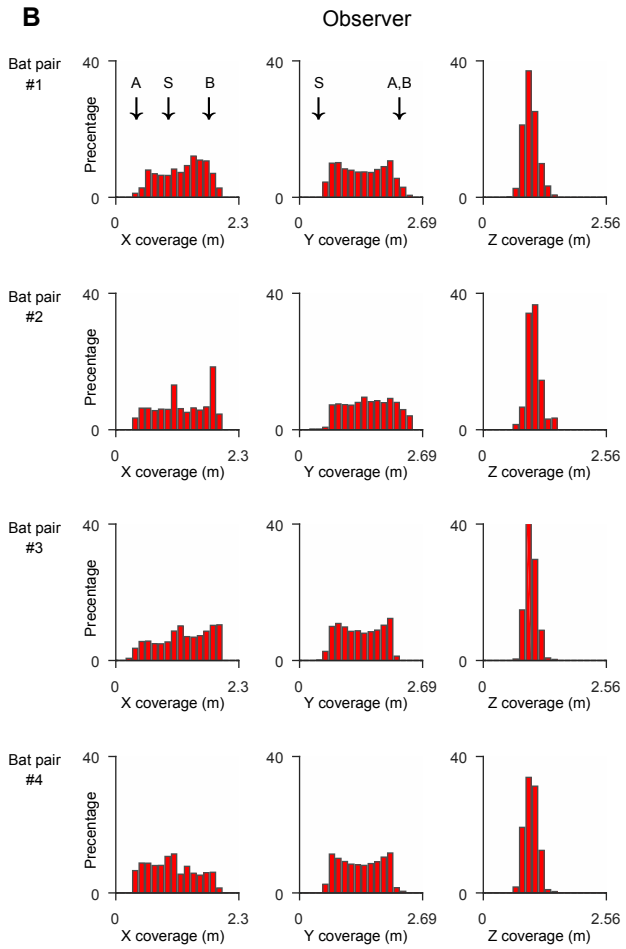
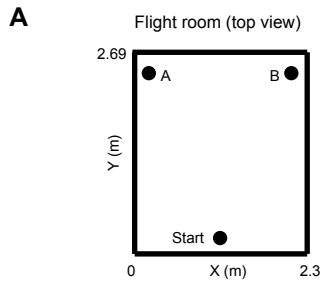
## **Histology and functional-anatomy**

Histology was done as described previously (6, 9). In brief, at the end of recordings, the implanted bats were anesthetized, and electrolytic lesions (DC positive current of 30  $\mu$ A, 15-s duration) were made to assist in the precise reconstruction of tetrode positions. The bat was then given an overdose of sodium pentobarbital and, with tetrodes left *in situ*, was perfused transcardially using 4% paraformaldehyde or 4.5% histofix. The brain was removed and thin coronal sections were cut at 30- $\mu$ m intervals. The sections were Nissl-stained with cresyl violet and were photographed to determine the locations of tetrode tracks in dorsal CA1.

To reconstruct the proximodistal and longitudinal positions of tetrode tracks within CA1 (fig. S7 and Fig. 4H), we created a 3D model of bat CA1 in stereotaxic coordinates, by measuring CA1 shape on each plate of the *Egyptian fruit bat atlas in stereotaxic coordinates* (R. Eilam et al., in preparation), and concatenating them in 3D. This allowed us to identify the longitudinal axis of CA1 (which is oriented 53° away from the midline) and the proximodistal axis (which is transverse to the longitudinal axis). We then transformed the measured position of each tetrode-track into common atlas coordinates, and then computed the position of the tetrode-track in longitudinal and proximodistal coordinates within CA1 – using the 3D model of CA1. The proximodistal coordinate was measured along the curved 3D surface of CA1, with 0 corresponding to the CA1-CA2 border. The longitudinal coordinate was measured as the horizontal distance from the CA1 septal pole. We included in the analysis in Fig. 4H data from the 1 bat which met our inclusion criteria, namely: 4 tetrodes with >20 cells per tetrode, and a good span of the tetrode-track positions along the proximodistal axis (see fig. S7). We grouped the data from the 2 proximal tetrodes into the ‘Proximal’ bars in Fig. 4H, and the data from the 2

more distal tetrodes into the 'Distal' bars in Fig. 4H. We then used the log-odds ratio statistical test to compare the ratios of significant cells between proximal and distal tetrodes (see Fig. 4H).

# Supplementary figure 1 - page 1



Continued on the next page -->

## Supplementary figure 1 - page 2

**fig. S1. Bats flew primarily in the horizontal plane, within a restricted horizontal slab.** (A) Schematic top-view on the flight room. (B and C) Distribution of behavioral coverage for the observer bat (B) and demonstrator bat (C), during flight – showing the percentage of time spent by the bat at each location along the three dimensions of the room. Each row in B-C shows data from one day; different rows are from different bat-pairs. Left column, behavioral coverage in the X dimension of the room (X-size of the room: 2.30 m); middle column, for the Y dimension (Y-size: 2.69 m); right column, for the Z dimension (Z-size: 2.56 m). Arrows above the top row indicate the locations of the landing-balls (ball ‘A’ and ball ‘B’) and the start-ball (‘S’). Note that in this behavioral setup the distributions in X and Y were relatively uniform – while in the Z dimension (height) the distribution was much less uniform, and was concentrated around the Z-height of the landing-balls – demonstrating that the bats flew in a rather narrow horizontal slab in the X-Y plane. (D and E) Population quantification of the uniformity of coverage in X and Y, and the ‘peakiness’ (narrow distribution) of coverage in Z for the observer bats (D) and demonstrator bats (E): Plotted is the ratio between the maximum height of the histogram divided by the mean height of the histogram. Error-bars, population average  $\pm$  s.e.m., pooling over all bats and all days in which we recorded well-separated neurons (total  $n = 290$  recording days across 4 pairs of bats). The ratio in the Z dimension was significantly higher than in the other two dimensions (Panel D:  $t$ -test comparing Z and Y:  $P < 10^{-98}$ ;  $t$ -test comparing Z and X:  $P < 10^{-70}$ ; Panel E:  $t$ -test comparing Z and Y:  $P < 10^{-111}$ ;  $t$ -test comparing Z and X:  $P < 10^{-72}$ ).

## Supplementary figure 2

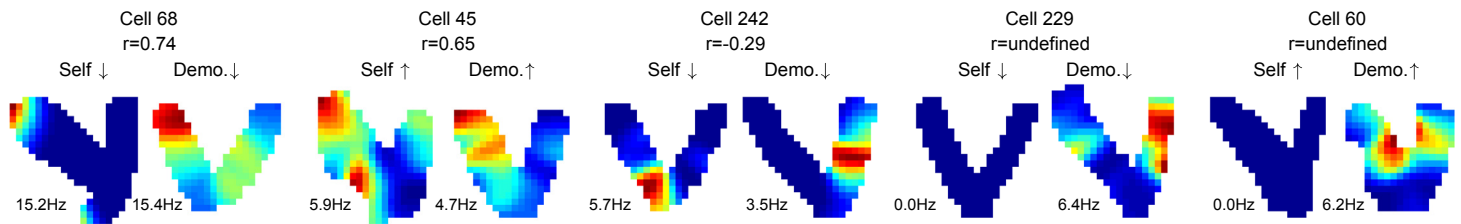
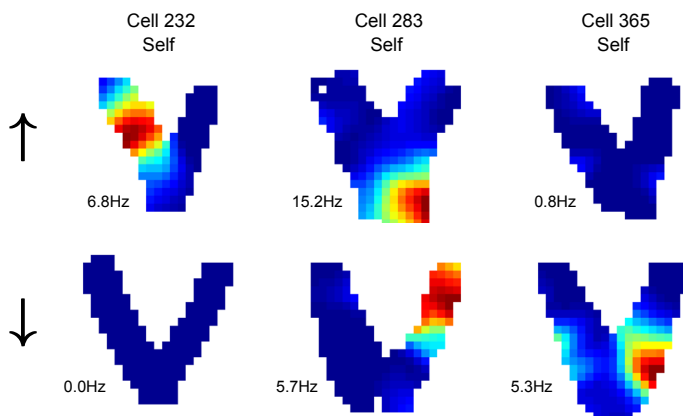


**fig. S2. Additional examples of social place-cells.** For each neuron, two firing-rate maps are plotted. Left: The classical firing-rate map based on the observer-bat own flights ('self' map). Right: the non-standard firing-rate map based on correlating the activity of the neuron in the observer's CA1 with the flight trajectories of the demonstrator bat ('Demo.' map). Color-scale ranges from zero (blue) to maximal firing-rate (red; value indicated). The Pearson correlation between the self-map and demonstrator-map is indicated for each cell (correlations are undefined for cells 229 and 60 because one of the maps is flat). Arrows denote the flight-direction ( $\uparrow$ , flying away from the start-ball;  $\downarrow$ , flying towards the start-ball).

## Supplementary figure 3

**A**



**B**

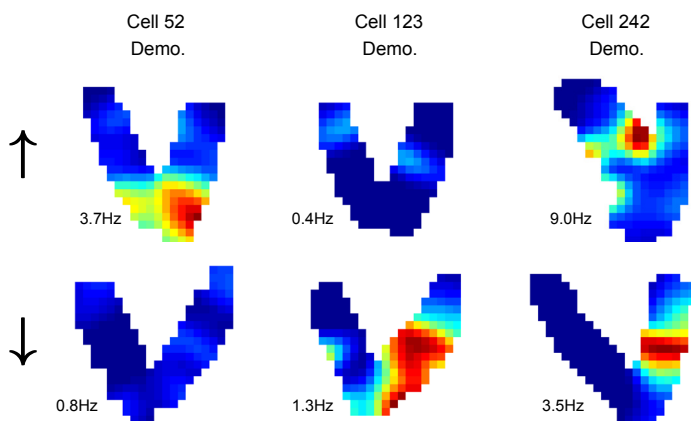


### fig. S3. Examples of directionality in the maps for self and other.

(A) Classical place cells: Shown are three example self place-cells exhibiting directional selectivity. Top, firing-rate maps calculated using flights directed from the start-ball to landing-balls A and B ( $\uparrow$ ). Bottom, firing-rate maps calculated using flights directed back to the start-ball ( $\downarrow$ ). (B) Social place-cells: Shown are three example social place-cells exhibiting directional selectivity. Same graphical convention as in panel A.

## Supplementary figure 4

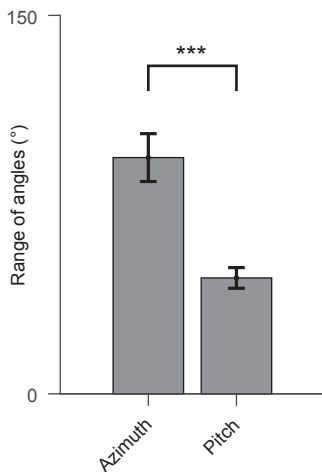


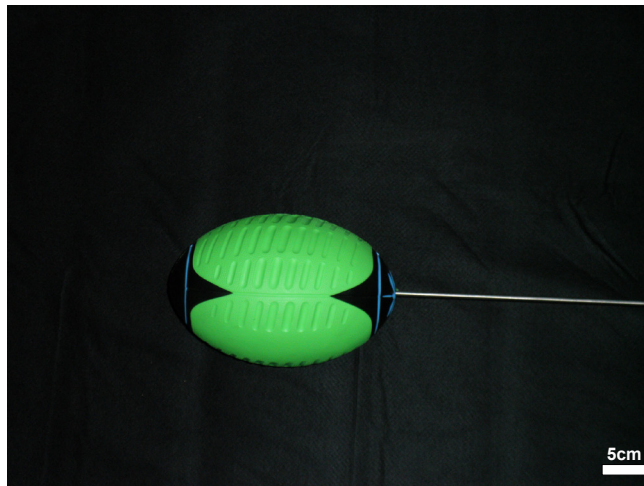
**fig. S4. The observer bat moved its head mainly in azimuth, in the horizontal plane.** This plot shows the range of angles covered by the bat's head in azimuth (left) and in pitch (right), over an entire recording-day – averaged across all recording-days which had motion sensor recordings ( $n = 18$  days; error bars, mean  $\pm$  s.e.m.). The range of angles for each day was defined as the 10–90 percentile range of head-azimuth and head-pitch, respectively; the range-of-angles was computed only for time-epochs when the demonstrator-bat was flying and the observer-bat was stationary on the start-ball. Note that although the observer-bats did not move their head much *during* the demonstrator's flights, their head did point in different azimuthal directions *across* different flights within a session – and therefore the bat covered a broad overall range of azimuthal angles (left bar); by contrast, the range of pitch angles was narrower ( $t$ -test:  $P < 10^{-5}$ ) – demonstrating that the bat moved its head across trials primarily in azimuth. Therefore, in Fig. 2B-F and Fig. 3 we restricted our analyses of head-direction to the azimuthal direction (horizontal plane). Another important reason for focusing on the azimuth was that the behavioral task itself was restricted mainly to the horizontal plane (fig. S1).

## Supplementary figure 5

### A. Demonstrator bat



### B. Informative object



### C. Noninformative object



**fig. S5. Bat and inanimate objects used for the experiment in Fig. 4. (A)** Egyptian fruit bat in flight. **(B)** Informative object. **(C)** Noninformative object. Scale bars, 5 cm.

## Supplementary figure 6 - page 1

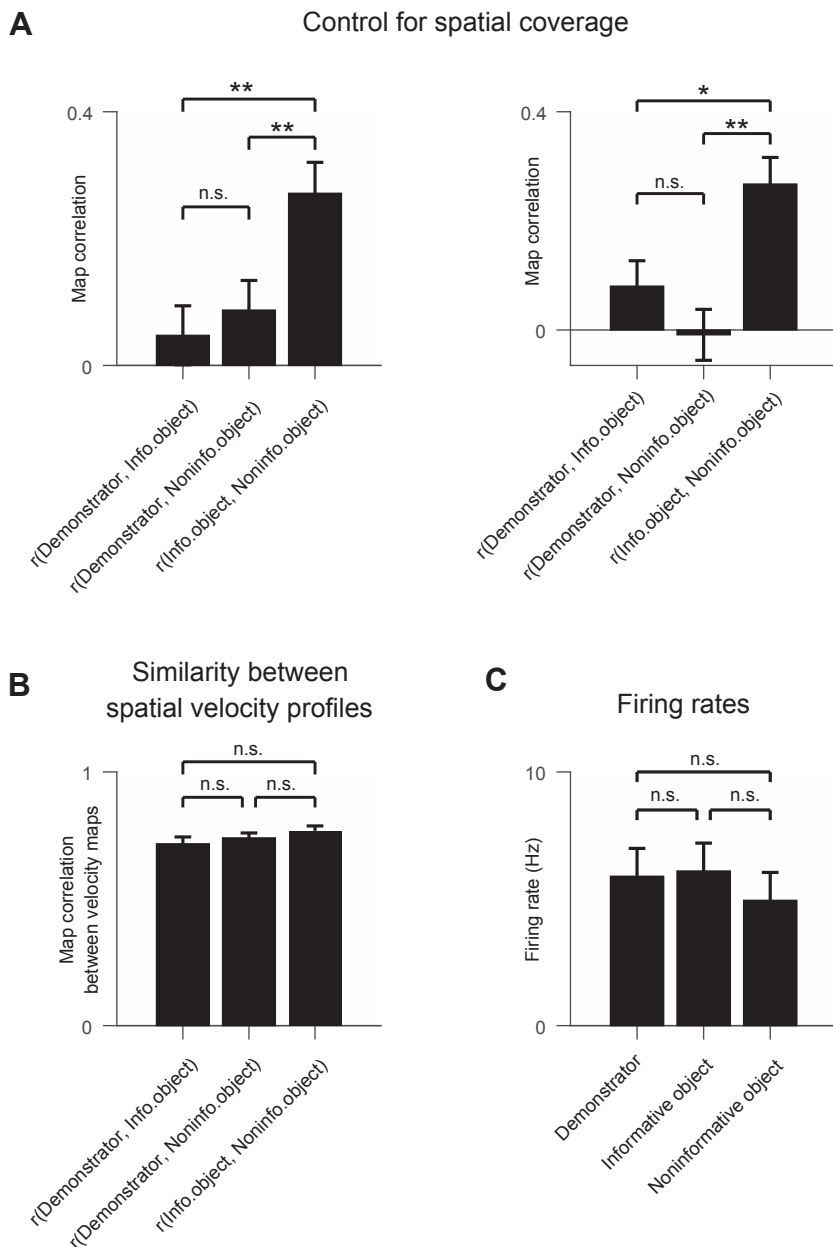


**fig. S6.** The observed differences in the representation of the conspecific bat versus the representations of objects cannot be explained by differences in 3D spatial coverage, or in velocity profiles, or in firing-rates. **(A)** Control for spatial-coverage. Left: Map correlations between the firing-rate maps of demonstrator-bat versus informative-object (left bar); between demonstrator-bat and noninformative-object (middle bar); and between informative-object and noninformative-object (right bar). Same as in Fig. 4G, but here we controlled for 3D spatial coverage, by computing the correlations only using the overlapping 3D-voxels between each pair of maps. Right: Same control for overlapping-3D-voxels – but computed only for maps with >40% overlap. Error bars, mean  $\pm$  s.e.m.; ‘\*’,  $P < 0.05$ ; ‘\*\*’,  $P < 0.01$ ; ‘n.s.’, non-significant. Note that these graphs are rather similar to Fig. 4G – suggesting that differences in spatial coverage cannot account for the results in Fig. 4G.

Continued on next page -->

## Supplementary figure 6 - page 2

**(B)** Control for velocity-profiles. For this analysis, we computed the spatial distribution of flight-velocity for each session ('velocity map'), using the same spatial binning and same smoothing as we used for the neural firing-rate maps. We then asked whether the similarities between velocity maps might explain the similarities between neural maps. Here we plotted the similarity (map correlation) between the spatial velocity maps for the demonstrator-bat versus informative-object (left bar), for demonstrator-bat versus noninformative-object (middle bar), and for informative-object versus noninformative-object (right bar) – for the same data as in Fig. 4G. Error bars, mean  $\pm$  s.e.m. Note that all these differences were non-significant (n.s.) – suggesting that differences in velocity maps cannot account for the results in Fig. 4G. **(C)** Control for firing-rates. Peak firing-rates for neurons significantly tuned to the demonstrator-bat (left bar,  $n = 45$  maps  $\times$  directions), to informative object (middle bar,  $n = 53$  maps  $\times$  directions) and to noninformative object (right bar,  $n = 58$  maps  $\times$  directions). Error bars, mean  $\pm$  s.e.m. Note that all these differences were non-significant (n.s.) – suggesting that differences in peak firing-rates cannot account for the results in Fig. 4G. (Firing-rates for the demonstrator-bat were computed in panel C only for neurons recorded in the 2 bats where we also conducted the recording-sessions with objects – unlike Fig. 1G, where the firing-rates were computed over neurons from all 4 bats; hence the firing-rates for the demonstrator maps were slightly different here from Fig. 1G.). Panels A,B,C here included only cells that met a strict criterion of  $>25$  flights per map and  $>50$  spikes per map – same criteria as in Fig. 4C,D,F,G.

## Supplementary figure 7

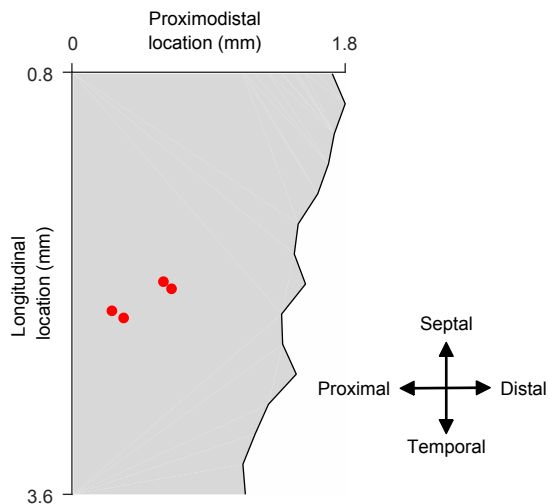


**fig. S7. Positions of four tetrode penetrations in dorsal CA1 of one animal.** The four tetrodes (red dots) were projected onto the CA1 longitudinal coordinates (position along the long axis of the hippocampus) and proximodistal coordinates (perpendicular to the long axis) (14). 'Proximal' means here close to CA2, and 'distal' means close to Subiculum. The vertical line on the left marks the CA1-CA2 border, while the thick jagged line on the right marks the CA1-Subiculum border. The data from these tetrodes were analyzed in Fig. 4H, separately for the two proximal tetrodes (denoted 'proximal' in Fig. 4H) and the two distal tetrodes ('distal' in Fig. 4H).

## Supplementary figure 8

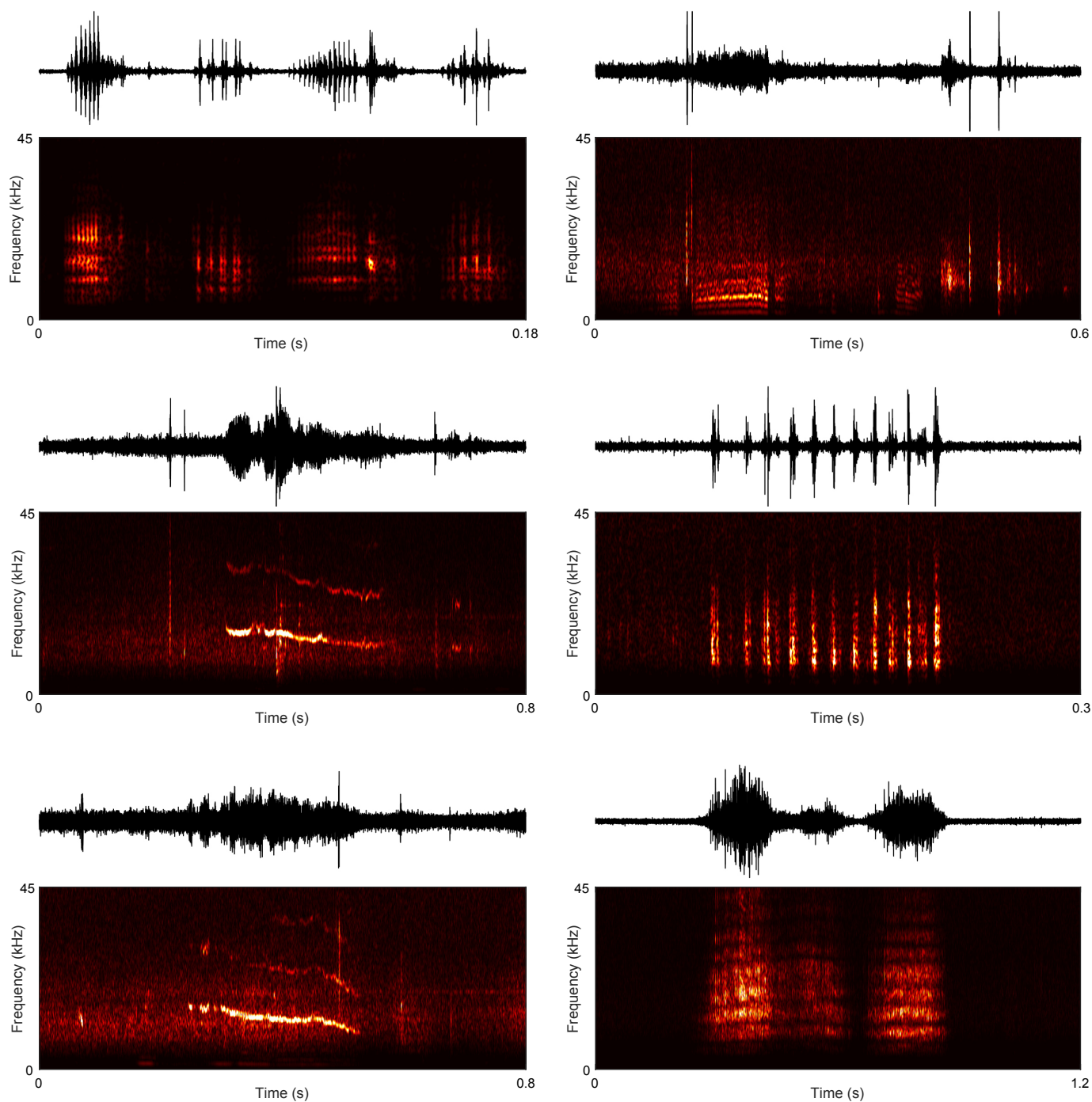


**fig. S8. Observer and demonstrator bats displayed rich vocal interactions.** Six different examples are shown for social vocalizations that were recorded during session 1. Top: Time-course of the sound signal. Bottom: time-frequency plot showing the spectrogram of the social vocalization; spectrograms show a frequency band of 0–45 kHz; bright color indicates high intensity (linear scale). Data taken from the last 2 pairs of bats (same bats as in Fig. 4).

## Supplementary Movie Legends

**Supplementary Movie 1:** A movie that illustrates schematically the delayed match-to-place task. Blue color, demonstrator bat. Red color, observer bat (this bat was implanted with a microdrive and equipped with a neural-logger for wireless neural recordings). Bats and landing-balls are not drawn to scale, for illustration purposes.

**Supplementary Movie 2:** A movie showing video-tracking of the two bats as captured through one of the two cameras in the experiment. Light-emitting diodes (LEDs) were placed on the bats' heads, and were used for tracking. Blue LED, demonstrator bat; Red LED, observer bat. Video-tracker image was smoothed for clarity. Note that the observer bat mimicked the flight-targets of the demonstrator-bat (ball A or ball B): In the first trial the demonstrator bat (blue) flew to ball B (right), and after a delay the observer bat (red) mimicked it and also flew to ball B; subsequently, the demonstrator bat flew to ball A (left), and the observer bat (red) mimicked it again and flew to ball A. Movie sped-up 2x.

## References and Notes

1. J. O'Keefe, L. Nadel, *The Hippocampus as a Cognitive Map* (Oxford Univ. Press, 1978).
2. M. A. Wilson, B. L. McNaughton, Dynamics of the hippocampal ensemble code for space. *Science* **261**, 1055–1058 (1993). [doi:10.1126/science.8351520](https://doi.org/10.1126/science.8351520) [Medline](#)
3. N. Ulanovsky, C. F. Moss, Hippocampal cellular and network activity in freely moving echolocating bats. *Nat. Neurosci.* **10**, 224–233 (2007). [doi:10.1038/nn1829](https://doi.org/10.1038/nn1829) [Medline](#)
4. T. Hafting, M. Fyhn, S. Molden, M.-B. Moser, E. I. Moser, Microstructure of a spatial map in the entorhinal cortex. *Nature* **436**, 801–806 (2005). [doi:10.1038/nature03721](https://doi.org/10.1038/nature03721) [Medline](#)
5. C. Barry, R. Hayman, N. Burgess, K. J. Jeffery, Experience-dependent rescaling of entorhinal grids. *Nat. Neurosci.* **10**, 682–684 (2007). [doi:10.1038/nn1905](https://doi.org/10.1038/nn1905) [Medline](#)
6. M. M. Yartsev, M. P. Witter, N. Ulanovsky, Grid cells without theta oscillations in the entorhinal cortex of bats. *Nature* **479**, 103–107 (2011). [doi:10.1038/nature10583](https://doi.org/10.1038/nature10583) [Medline](#)
7. J. S. Taube, R. U. Muller, J. B. Ranck Jr., Head-direction cells recorded from the postsubiculum in freely moving rats. I. Description and quantitative analysis. *J. Neurosci.* **10**, 420–435 (1990). [Medline](#)
8. A. Peyrache, M. M. Lacroix, P. C. Petersen, G. Buzsáki, Internally organized mechanisms of the head direction sense. *Nat. Neurosci.* **18**, 569–575 (2015). [doi:10.1038/nn.3968](https://doi.org/10.1038/nn.3968) [Medline](#)
9. A. Finkelstein, D. Derdikman, A. Rubin, J. N. Foerster, L. Las, N. Ulanovsky, Three-dimensional head-direction coding in the bat brain. *Nature* **517**, 159–164 (2015). [doi:10.1038/nature14031](https://doi.org/10.1038/nature14031) [Medline](#)
10. T. Solstad, C. N. Boccara, E. Kropff, M.-B. Moser, E. I. Moser, Representation of geometric borders in the entorhinal cortex. *Science* **322**, 1865–1868 (2008). [doi:10.1126/science.1166466](https://doi.org/10.1126/science.1166466) [Medline](#)
11. F. Savelli, D. Yoganarasimha, J. J. Knierim, Influence of boundary removal on the spatial representations of the medial entorhinal cortex. *Hippocampus* **18**, 1270–1282 (2008). [doi:10.1002/hipo.20511](https://doi.org/10.1002/hipo.20511) [Medline](#)
12. C. Lever, S. Burton, A. Jeewajee, J. O'Keefe, N. Burgess, Boundary vector cells in the subiculum of the hippocampal formation. *J. Neurosci.* **29**, 9771–9777 (2009). [doi:10.1523/JNEUROSCI.1319-09.2009](https://doi.org/10.1523/JNEUROSCI.1319-09.2009) [Medline](#)
13. G. Neuweiler, *The Biology of Bats* (Oxford Univ. Press, 2000).
14. Materials and methods are available as supplementary materials.
15. M. M. Yartsev, N. Ulanovsky, Representation of three-dimensional space in the hippocampus of flying bats. *Science* **340**, 367–372 (2013). [doi:10.1126/science.1235338](https://doi.org/10.1126/science.1235338) [Medline](#)
16. B. E. Pfeiffer, D. J. Foster, Autoassociative dynamics in the generation of sequences of hippocampal place cells. *Science* **349**, 180–183 (2015). [doi:10.1126/science.aaa9633](https://doi.org/10.1126/science.aaa9633) [Medline](#)

17. J. Ferbinteanu, M. L. Shapiro, Prospective and retrospective memory coding in the hippocampus. *Neuron* **40**, 1227–1239 (2003). [doi:10.1016/S0896-6273\(03\)00752-9](https://doi.org/10.1016/S0896-6273(03)00752-9) [Medline](#)
18. T. J. Davidson, F. Kloosterman, M. A. Wilson, Hippocampal replay of extended experience. *Neuron* **63**, 497–507 (2009). [doi:10.1016/j.neuron.2009.07.027](https://doi.org/10.1016/j.neuron.2009.07.027) [Medline](#)
19. A. Sarel, A. Finkelstein, L. Las, N. Ulanovsky, Vectorial representation of spatial goals in the hippocampus of bats. *Science* **355**, 176–180 (2017). [doi:10.1126/science.aak9589](https://doi.org/10.1126/science.aak9589) [Medline](#)
20. S. A. Ho, E. Hori, T. Kobayashi, K. Umeno, A. H. Tran, T. Ono, H. Nishijo, Hippocampal place cell activity during chasing of a moving object associated with reward in rats. *Neuroscience* **157**, 254–270 (2008). [doi:10.1016/j.neuroscience.2008.09.004](https://doi.org/10.1016/j.neuroscience.2008.09.004) [Medline](#)
21. E. J. Henriksen, L. L. Colgin, C. A. Barnes, M. P. Witter, M.-B. Moser, E. I. Moser, Spatial representation along the proximodistal axis of CA1. *Neuron* **68**, 127–137 (2010). [doi:10.1016/j.neuron.2010.08.042](https://doi.org/10.1016/j.neuron.2010.08.042) [Medline](#)
22. A. Tsao, M.-B. Moser, E. I. Moser, Traces of experience in the lateral entorhinal cortex. *Curr. Biol.* **23**, 399–405 (2013). [doi:10.1016/j.cub.2013.01.036](https://doi.org/10.1016/j.cub.2013.01.036) [Medline](#)
23. J. J. Knierim, J. P. Neunuebel, S. S. Deshmukh, Functional correlates of the lateral and medial entorhinal cortex: Objects, path integration and local-global reference frames. *Philos. Trans. R. Soc. Lond. B Biol. Sci.* **369**, 20130369 (2013). [doi:10.1098/rstb.2013.0369](https://doi.org/10.1098/rstb.2013.0369) [Medline](#)
24. F. L. Hitti, S. A. Siegelbaum, The hippocampal CA2 region is essential for social memory. *Nature* **508**, 88–92 (2014). [doi:10.1038/nature13028](https://doi.org/10.1038/nature13028) [Medline](#)
25. S. M. Dudek, G. M. Alexander, S. Farris, Rediscovering area CA2: Unique properties and functions. *Nat. Rev. Neurosci.* **17**, 89–102 (2016). [doi:10.1038/nrn.2015.22](https://doi.org/10.1038/nrn.2015.22) [Medline](#)
26. T. Okuyama, T. Kitamura, D. S. Roy, S. Itohara, S. Tonegawa, Ventral CA1 neurons store social memory. *Science* **353**, 1536–1541 (2016). [doi:10.1126/science.aaf7003](https://doi.org/10.1126/science.aaf7003) [Medline](#)
27. L. Zynnyuk, J. Huxter, R. U. Muller, S. E. Fox, The presence of a second rat has only subtle effects on the location-specific firing of hippocampal place cells. *Hippocampus* **22**, 1405–1416 (2012). [doi:10.1002/hipo.20977](https://doi.org/10.1002/hipo.20977) [Medline](#)
28. M. von Heimendahl, R. P. Rao, M. Brecht, Weak and nondiscriminative responses to conspecifics in the rat hippocampus. *J. Neurosci.* **32**, 2129–2141 (2012). [doi:10.1523/JNEUROSCI.3812-11.2012](https://doi.org/10.1523/JNEUROSCI.3812-11.2012) [Medline](#)
29. X. Mou, D. Ji, Social observation enhances cross-environment activation of hippocampal place cell patterns. *eLife* **5**, e18022 (2016). [doi:10.7554/eLife.18022](https://doi.org/10.7554/eLife.18022) [Medline](#)
30. E. J. Markus, Y. L. Qin, B. Leonard, W. E. Skaggs, B. L. McNaughton, C. A. Barnes, Interactions between location and task affect the spatial and directional firing of hippocampal neurons. *J. Neurosci.* **15**, 7079–7094 (1995). [Medline](#)
31. M. A. Moita, S. Rosis, Y. Zhou, J. E. LeDoux, H. T. Blair, Hippocampal place cells acquire location-specific responses to the conditioned stimulus during auditory fear conditioning. *Neuron* **37**, 485–497 (2003). [doi:10.1016/S0896-6273\(03\)00033-3](https://doi.org/10.1016/S0896-6273(03)00033-3) [Medline](#)

32. H. Eichenbaum, N. J. Cohen, Can we reconcile the declarative memory and spatial navigation views on hippocampal function? *Neuron* **83**, 764–770 (2014). [doi:10.1016/j.neuron.2014.07.032](https://doi.org/10.1016/j.neuron.2014.07.032) [Medline](#)
33. G. Rizzolatti, C. Sinigaglia, The mirror mechanism: A basic principle of brain function. *Nat. Rev. Neurosci.* **17**, 757–765 (2016). [doi:10.1038/nrn.2016.135](https://doi.org/10.1038/nrn.2016.135) [Medline](#)
34. A. Tuval, N. Ulanovsky, L. Las, T. Bdolah-Abram, Y. Shilo-Benjamini, in *Federation of Laboratory Animal Science Associations* (2016).
35. X. Yun, E. R. Bachmann, R. B. McGhee, *IEEE Trans. Instrum. Meas.* **57**, 638–650 (2008). [doi:10.1109/TIM.2007.911646](https://doi.org/10.1109/TIM.2007.911646)
36. M. D. Shuster, S. D. Oh, Three-axis attitude determination from vector observations. *J. Guid. Control* **4**, 70–77 (1981). [doi:10.2514/3.19717](https://doi.org/10.2514/3.19717)
37. W. E. Skaggs, B. L. McNaughton, M. A. Wilson, E. J. Markus, in *Advances in Neural Information Processing Systems 5*, S. J. Hanson, J. D. Cowan, C. L. Giles, Eds. (Morgan Kaufman, 1993), pp. 1030–1037.
38. A. K. Lee, M. A. Wilson, Memory of sequential experience in the hippocampus during slow wave sleep. *Neuron* **36**, 1183–1194 (2002). [doi:10.1016/S0896-6273\(02\)01096-6](https://doi.org/10.1016/S0896-6273(02)01096-6) [Medline](#)
39. D. J. Foster, M. A. Wilson, Reverse replay of behavioural sequences in hippocampal place cells during the awake state. *Nature* **440**, 680–683 (2006). [doi:10.1038/nature04587](https://doi.org/10.1038/nature04587) [Medline](#)
40. K. Diba, G. Buzsáki, Forward and reverse hippocampal place-cell sequences during ripples. *Nat. Neurosci.* **10**, 1241–1242 (2007). [doi:10.1038/nn1961](https://doi.org/10.1038/nn1961) [Medline](#)
41. G. Dragoi, S. Tonegawa, Preplay of future place cell sequences by hippocampal cellular assemblies. *Nature* **469**, 397–401 (2011). [doi:10.1038/nature09633](https://doi.org/10.1038/nature09633) [Medline](#)
42. B. E. Pfeiffer, D. J. Foster, Hippocampal place-cell sequences depict future paths to remembered goals. *Nature* **497**, 74–79 (2013). [doi:10.1038/nature12112](https://doi.org/10.1038/nature12112) [Medline](#)